Journal of the European Ceramic Society 22 (2002) 891–902

www.elsevier.com/locate/jeurceramsoc

Dried particle plasma spray in-flight synthesis of spinel coatings

G. Bertrand[a,*], C. Meunier[b], P. Bertrand[a], C. Coddet[a]

[a]*LERMPS, UTBM, Site de Sévenans, 90010 Belfort cedex, France*
[b]*CREST, Pôle Universitaire des Portes du Jura, BP 71427, 25211 Montbéliard cedex, France*

Received 15 December 2000; received in revised form 17 May 2001; accepted 3 June 2001

Abstract

Powder particle diameters currently used for spraying are generally between 5 and 100 μm with a preferred size range around 40–60 μm. Future trends in plasma spraying involve the use of fine or ultrafine powders and the reduction of the number of steps between raw material preparation and coating. The use of non-sintered spray dried ceramic aggregates as feedstock material for plasma spraying has accordingly been investigated. Al_2O_3 based coatings were prepared by this route of dried particle plasma spray (DPPS). The microstructure and crystallographic phases of these deposits were characterised using scanning electron microscopy (SEM) equipped with energy dispersive spectrometry (EDS) and X-ray diffraction (XRD). Given the intimate mixing of the starting oxides, reactions occur during spraying leading to the formation of spinel ($MgAl_2O_4$ and/or $ZnAl_2O_4$) and zinc aluminum oxide ($Zn_4Al_{22}O_{37}$). The layered structure of the deposit is characteristic of conventional plasma-sprayed coatings but the features are smaller in size. Depending on the operating conditions (plasma characteristics and powder injection), two different melting modes of the particles were identified; the first leads to individual well-melted droplets that splash regularly even if generating some fingers and the second leads to aggregates that are well-melted on their outer parts and strengthened in their cores.

Keywords: DPPS; $MgAl_2O_4$; Microstructure-final; Plasma spraying; $ZnAl_2O_4$

1. Introduction

Plasma spraying is a rapid heating, cooling and solidification process that often results in the formation of deposits characterised by a coarse grain structure, significant porosity (generally in the range 8–15 vol.%[1]) and a lamellar morphology.[2] Usually coarse structures are produced because spraying processes use coarse powders (20–90 μm) as feedstock materials. Furthermore, since the process is far from equilibrium, during spraying the feedstock material can be overheated in some parts and not molten in other parts. Therefore, changes from the original phase and chemical composition are observed over distances of a few micrometers in deposits produced by conventional powder plasma spraying (PPS). Of course, the properties of the deposits are directly related to their homogeneity both from the chemical and structural points of view.

In order to achieve chemically homogeneous coatings with finer and/or denser morphology, new spray processes have recently emerged. Among these, the suspension plasma spraying (SPS) technique uses a sol or a nanodispersed powder suspension as precursor.[3,4] This technology seems to facilitate chemical reactions between the components intimately mixed into the suspension. Meanwhile, the vaporisation of the liquid used as a medium for the suspension cools the plasma, less thermal energy is therefore available for the melting of the conveyed solid. This results in high values of porosity and incomplete reaction between the components. Other processes as liquid flame spray (LFS) and plasma spraying of liquid precursors (PSLP) are based on metal-organic or aqueous liquid precursors as feedstock materials.[5–7] Droplets of the atomised liquid feedstock are injected in the hot zone of the combustion flame or plasma jet and lead to the formation of nanoparticles. By using the so-produced nanoparticles as in situ feedstock material it is possible to produce nanograined coatings. To the authors' knowledge, the flame spray synthesis process was found until now to be more suitable for producing powders than deposits. Indeed, the deposition efficiency of the coatings appears generally to be lower than 10% and coatings have a rather powdery structure. Finally, small-particle plasma spray (SPPS) is

* Corresponding author. Tel.: +33-3-84-58-3240; fax: +33-3-84-58-3286.
E-mail address: ghislaine.bertrand@utbm.fr (G. Bertrand).

0955-2219/02/$ - see front matter
PII: S0955-2219(01)00381-8

a process by which particles as fine as 40 nm can be sprayed.[8] The SPPS process relies on a special injector technology. Al_2O_3 coatings prepared using this new process exhibit a layered structure, characteristic of conventional plasma-sprayed coatings, but smaller in feature size with fine cavities and microcracks.

In this paper, we describe the morphology and crystalline structures of coatings resulting from a new plasma spray route by which non-sintered spray-dried particles are directly introduced in the plasma spray torch. The present study was especially focused on the chemical and physical behaviour of agglomerated granules inside a dc plasma torch. The dried particle plasma spray (DPPS) process is expected to combine the advantages of the previously mentioned new processes (suspension or liquid plasma spray and small particle plasma spray). Indeed, the DPPS process makes it possible at the same time to achieve thin structures with competitive deposition efficiencies since it is based on solid precursors and to complete in-flight chemical reactions since the initial components are of small size and are intimately mixed. The $Mg(OH)_2{\cdot}ZnO{\cdot}Al_2O_3$ mixture was used as precursor for the evaluation of the DPPS process. Spinel is ideally suited as model component in extended alumina systems. It is the principal constituent in the (MgO or ZnO)/Al_2O_3 phase diagrams. With a high melting temperature (2135 °C) and a low thermal conductivity (15 W mK^{-1}), spinel ($MgAl_2O_4$) coatings have been exploited for various applications in chemical engineering and steel production.[9–13] For instance, such coatings are used for the protection of metal alloys against hot corrosion and oxidation from fused metal or glass and for the minimisation of wear damage. It is also a candidate material for insulating coatings because of its high electrical and radiation resistivity.

The results reported here represent a first attempt to investigate dried particle plasma spray as a potential processing route for depositing ceramic coatings with thinner structures (lamellae and pores). To control the coating build up, it was necessary to investigate the changes undergone by the powder from its starting state to the splats constituting the coating. The crystallographic structure and the morphology of mixture of oxides were assessed at each step of the plasma spray process, e.g. before spraying (starting agglomerated powder), during plasma crossing (powder melting and changes), during impact (splat formation) and during splat stacking up (coating completed). The characterisations have been performed to identify the shape changes by scanning electron microscopy and the crystalline phases or grain size modifications by X-ray diffraction.

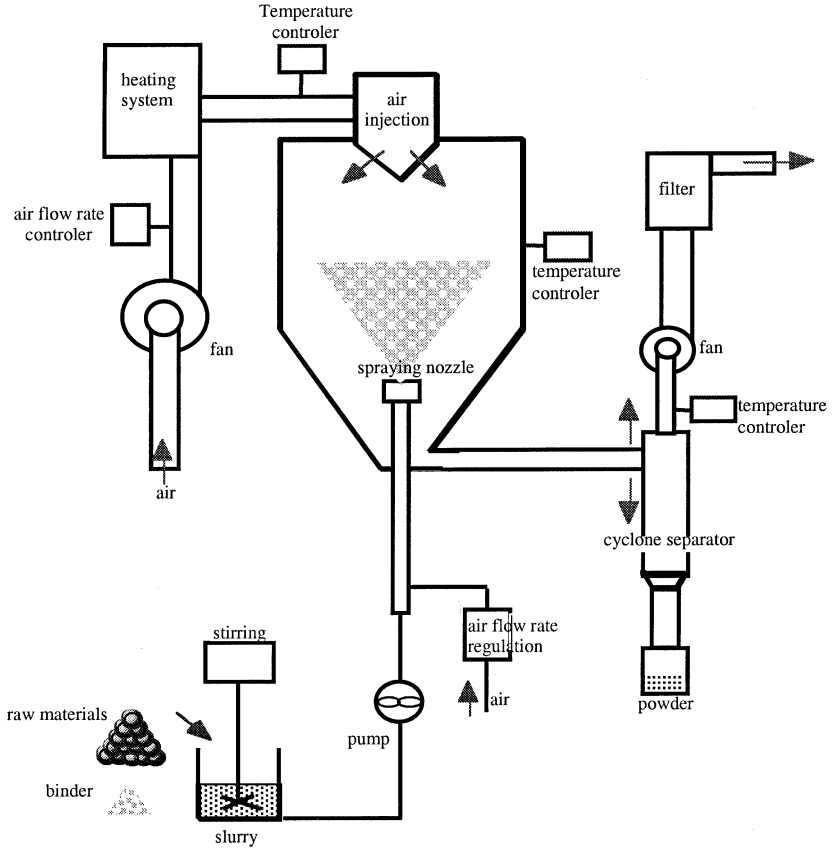

Fig. 1. A schematic view of the spray dryer apparatus designed and built in the laboratory.

2. Experimental procedures

2.1. Powder fabrication

The spray drying process[14] consists at spraying slurry containing finely dispersed particles of the materials to be agglomerated, organic compounds and water. Fig. 1 gives a schematic view of the spray dryer apparatus designed, fabricated and used in the laboratory. It is a non-commercial apparatus, which principle is based on counter-current reactor. A peristaltic pump feeds the slurry into a two-fluid nozzle atomiser designed with a special geometry to generate a vortex of the fluid. The atomised slurry is thrown using a fountain mode into a large cyclone like chamber in a counter-current stream of heated air. The moisture contained in the droplets evaporates during their flight in the chamber. The resulting solid granulates are collected at the bottom of the chamber and are separated from the gas in cyclone collectors.

The formulation of the slurry includes fine Al_2O_3 (P152SB from Aluminium Pechiney, size below 5 μm), ZnO and $Mg(OH)_2$ (from Lambert Rivière S.A., size inferior to 1 μm) particles as raw materials, acrylic copolymer (Coatex) as surfactant, polyvinyl alcohol (Rhodia) as binder and additives (alcohol from Prolabo). The detailed composition of the alumina-based slurry employed in this work is reported in Table 1.

The main controlled spray parameters are the air temperature (at the entry, exit and inside the chamber), the atomizing nozzle design and the atomising air and slurry flow rates. The conditions used in this study are reported in Table 2 and correspond to a slurry feed rate of 1kg/min. The ambient air temperature achieved in the spray dryer chamber leads to a rapid evaporation of the liquid phase.

Table 1
Formulation of the slurry used for the spray-drying (numbers are wt.%)

Slurry	Composition	
Solids	Al_2O_3	58.1%
	$Mg(OH)_2$	16.6%
	ZnO	23.2%
Binder		1.7%
Surfactant		0.5%
Additives		2.9%

Table 2
Spray-drying operating conditions used to realize SPI powders

Entry air temperature (°C)	225
Chamber air temperature (°C)	180
Exit air temperature (°C)	130
Atomizing air flow rate (m^3/h)	13–14

Granules with a diameter below 36 μm or between 36 and 63 μm were selected by mechanical sieving.

2.2. Coating

Two powder fractions (below 36 μm and 36–63 μm) were plasma sprayed with a Sulzer-Metco PT F4 torch in a closed room using a robot to ensure controlled and reproducible trajectories and speeds. The powder feeding system was a single bowl apparatus from Medicoat and the powder feed rate was fixed at 15 g/min. The XC10 steel substrates were sand blasted with corundum prior to spraying. During spraying, a cooling system consisting of liquid CO_2 jets was applied. This cooling system was already described elsewhere.[15] Approximately 200 μm thick deposits were formed after 8 passes of the torch.

In Table 3, the operating conditions are reported. Special attention was paid to the dependency of the microstructure and chemical composition of coatings on:

The nature of the plasma gas: Ar:H_2 or Ar:He
The power of the plasma jet: 16.5–22.5 kW
The carrier gas flow rate: 2–7 l min^{-1}
The injector angle: 70–90°.

2.3. Material characterization

The powder size distribution obtained after spray drying of this slurry was checked by laser light diffusion (Coulter LS130 from Beckman Coulter). In addition, a Fourier transform infra red spectrometer (from Nicolet) operating in the 4000–400 cm^{-1} range was employed to record the IR spectra using the KBr pellet technique. Approximately 1 mg of the studied sample were mixed with 150 mg of spectroscopic grade KBr and pressed into pellets. The FTIR spectroscopic studies were carried out on the alumina based samples both in the absence and in the presence of the binder.

The spinel structure, which has the general formula $A^{2+}B_2^{3+}O_4$, consists of an almost-perfect cubic close-packed oxygen arrangement in which the cations reside on tetrahedral and octahedral interstices. The space group is Fd3m. In the normal spinel structure, 8 tetrahedral sites (out of 64 in a unit cell) are occupied by divalent metal ions, whereas 16 octahedral sites (out of

Table 3
Coating conditions

Spraying parameters	
Ar:He or Ar:H_2 (%)	33:67 or 74:26
Current intensity (A)	450–750
Carrier gas (Ar / l min^{-1})	2–7
Injector angle (°)	70–90

32 in a unit cell) are occupied by trivalent metal ions. Natural crystals of magnesium aluminate spinel ($MgAl_2O_4$) have the normal structure in which Mg^{2+} ions are located at tetrahedral sites, Al^{3+} ions at octahedral sites.[16] Phase determination in the powders and the coatings was performed by X-ray diffraction (diffractometer X'pert MPD from Philips). The XRD patterns (Cu K_α) were recorded in the $\theta/2\theta$ mode either between 15 and 120° (2θ) with a step size of 0.05° (2θ) and a dwell time of 2 s/step or between 20 and 50° (2θ) with a step size of 0.02° (2θ) and a dwell time of 20 s/step. Because of the similarity of the crystalline structures, patterns were intricate as shown in Fig. 2 and a fitting analyse was always applied. Stoichiometric mixtures of $Mg(OH)_2$•Al_2O_3 and ZnO•Al_2O_3 were heat treated for 21 h at 1100 °C in an air furnace. The XRD patterns revealed that gahnite ($ZnAl_2O_4$) seems to be more easily produced than spinel ($MgAl_2O_4$).

The spray-dried powder morphology and the coating microstructure (polished surfaces and cross-sections and fractures) were observed by SEM (JSM 5800LV from Jeol).

3. Results and discussion

3.1. Powder feedstock characteristics

As observed by scanning electron microscopy, the spray-dried powder has a rather full spherical shape (as it is evidenced in Fig. 3a for powder with diameter below 36 μm) but some defaults such as elongated shapes are noticeable especially for the size range over 63 μm (Fig. 3b). For powder with diameter between 36 and 63 μm, heterogeneous structures were observed. Indeed, these granulates could consist of an outer rather regular part made of the elementary compounds and an inner part made of small agglomerated particles of 5–10 μm in diameter (Fig. 3c).

The apparent density varies from 0.899 g/cm^3 for powder diameter below 36 μm to 0.996 g/cm^3 for powder diameter between 36 and 63 μm.

On top of the mineral elementary components used to make the powder, the aggregates also contain organic compounds. The assignments of the various bands and peaks observed by FTIR are in accordance with those reported in the literature for similar functional groups.[17] The specific bands attributed to O–H stretching and bending are shifted towards lower values as shown on Fig. 4. This shift probably means that the organic molecules are linked to the solid particles by hydrogen bonds. In spite of such a weak connection, it appeared that the powder mechanical strength depending, to a degree, on the granule binder content was sufficient to allow its handling and injection in the plasma spraying torch according to the chosen conditions. However, it can be expected that the aggregates will separate to their elementary components when entering the plasma.

Plasma spray experiments were conducted to determine the influence of the plasma characteristics (plasma gas composition Ar:He and Ar:H_2 and plasma power from 16.5 to 22.5 kW) and the powder feeding conditions (carrier gas flow rate from 2 to 7 l min^{-1} and injector angle of 90 or 70°) on the chemical and morphological behaviour of this composite spray-dried powder. In plasma process, the key point is the melting stage of the powder. In order to study this step, powder was picked up after going past the plasma by spraying not onto a substrate but through a hole into a funnel placed at a distance of approximately 150 mm. These plasma-sprayed granules are called 'free-flight' particles.

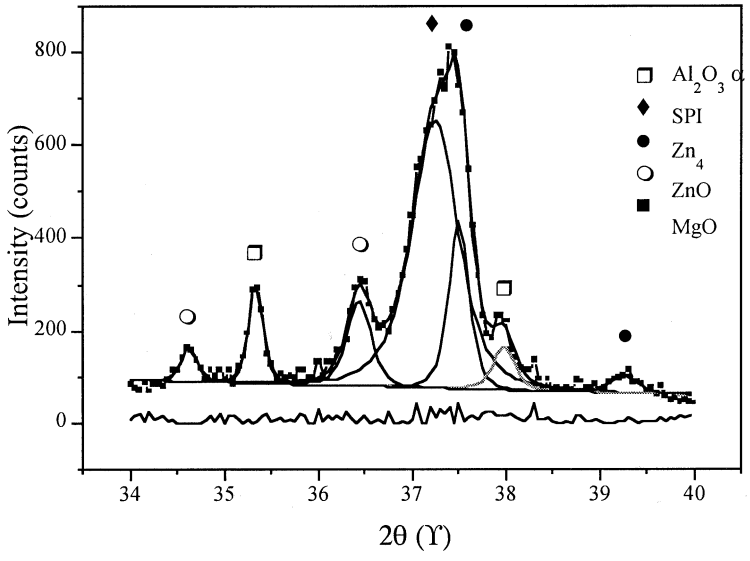

Fig. 2. Example of the fitted diffraction lines using modified lorentzian functions and a linear background.

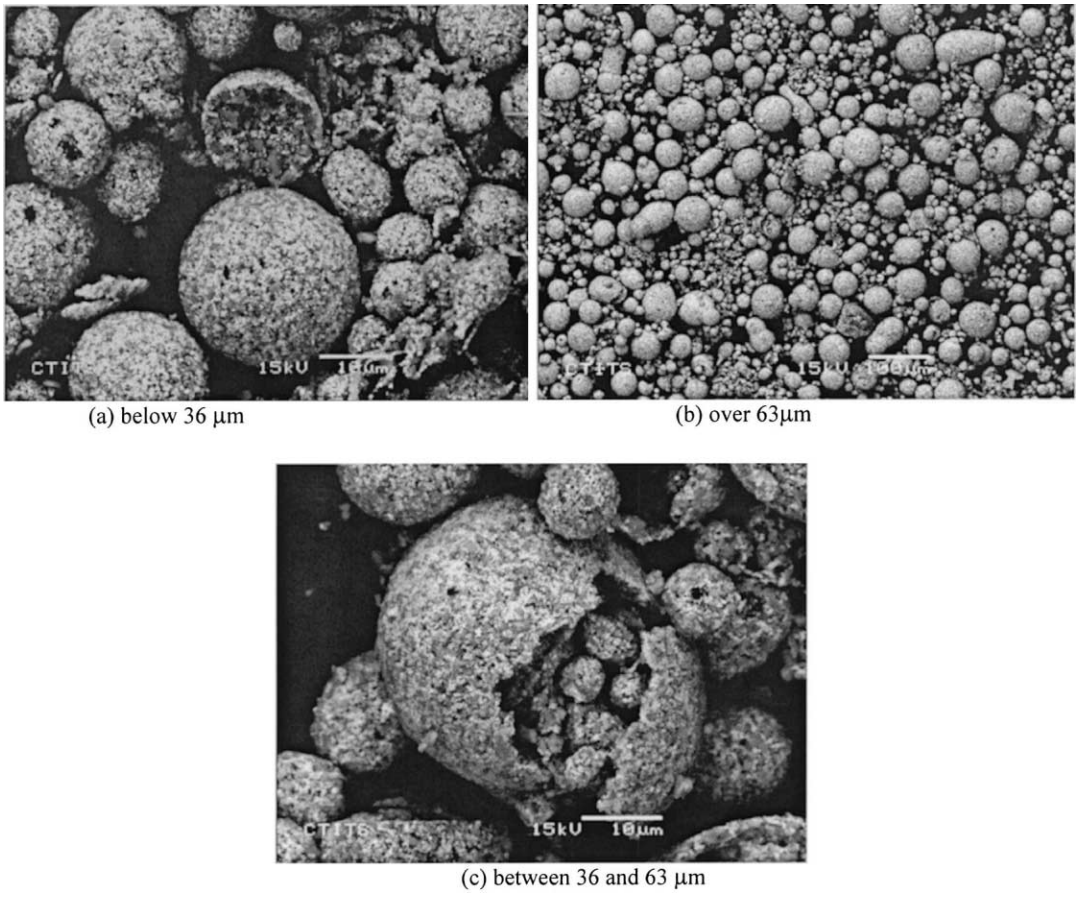

(a) below 36 µm (b) over 63µm

(c) between 36 and 63 µm

Fig. 3. SEM observation of as (non-sintered) spray dried powder aggregates with diameter below 36 µm (a), over 63 µm (b) and between 36 and 63 µm (c).

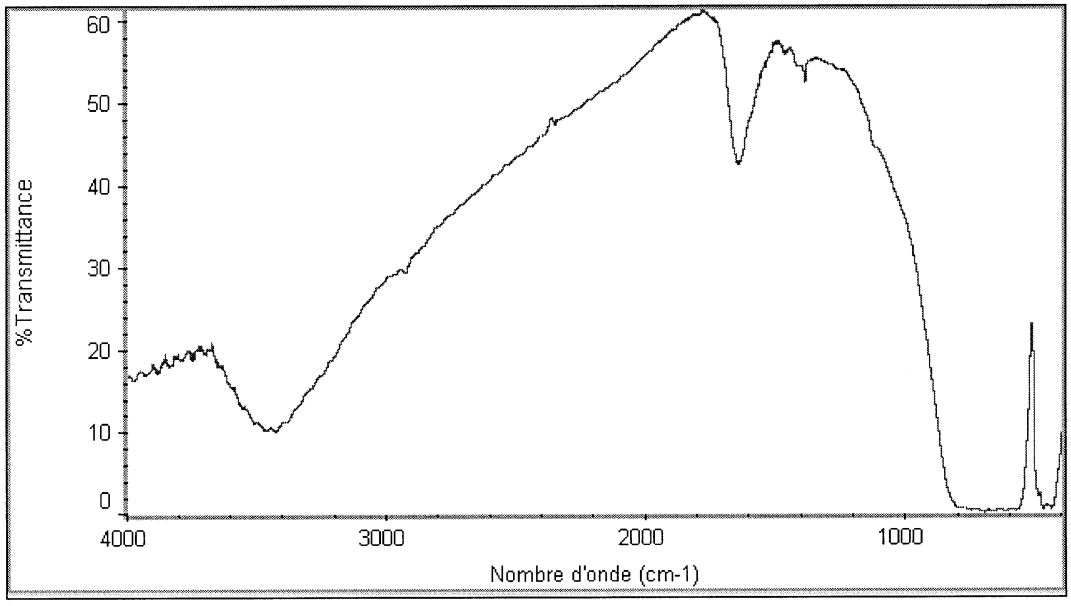

Fig. 4. FTIR spectrum of alumina-based powder agglomerated with PVA binder.

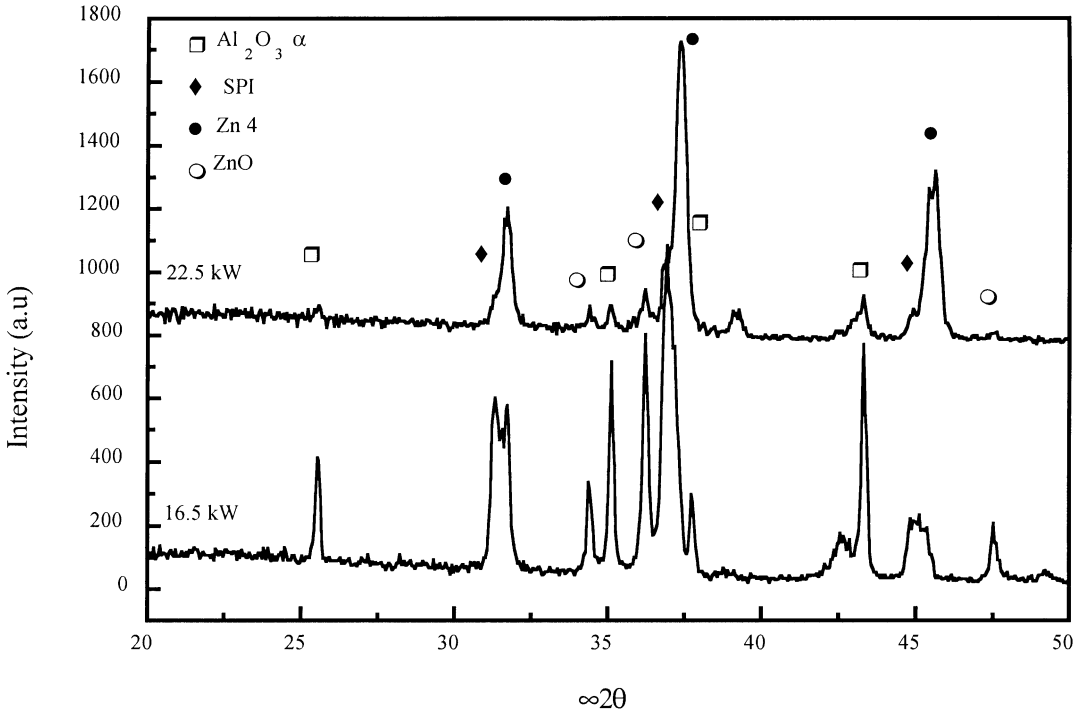

Fig. 5. $\theta/2\theta$ diffraction patterns of 'free-flight' powders sprayed in an Ar:H_2 plasma (a) at 16.5 kW and (b) at 22.5 kW.

3.2. Correlation between the melting degree and crystalline changes of the plasma sprayed aggregates

The XRD analysis of 'free-flight' powders show the presence of $MgAl_2O_4$ (spinel) and/or $ZnAl_2O_4$ (gahnite), both named 'SPI' in the following, and $Zn_4Al_{22}O_{37}$ (zinc aluminum oxide, named 'Zn_4') (Fig. 5). These compounds are the result of a reaction between the initial components, which degree of completion depends on the operating parameters as it will be demonstrated in the following. In addition, corundum (α-Al_2O_3), periclase (MgO) and zincite (ZnO, wurtzite) have also been pointed out in some XRD patterns, which is in accordance with the non-melted particles observed as can be seen on Fig. 6.

To assess the origin of Zn_4, SPI and α-Al_2O_3 phases, XRD analysis was also performed on a pure alumina coating realised in the same conditions (DPPS) as the multi-oxide deposit. It was found that the as-deposited coating consists of α-Al_2O_3 and γ-Al_2O_3.

$$\begin{array}{lll} \alpha\text{-}Al_2O_3 & \longrightarrow & \alpha\text{-}Al_2O_3 \\ (675\,\text{Å}/0.2\%) & & (1975\,\text{Å}/0.1\%) \end{array}$$

$$\begin{array}{lll} & + \gamma\text{-}Al_2O_3 & \text{phase} \\ & (265\,\text{Å}/0.7\%) & \text{grain size/strain \%} \end{array}$$

The presence of the γ phase can be explained on the basis of nucleation kinetics; γ-Al_2O_3 is more easily nucleated from the melt than α-Al_2O_3 because of a lower interfacial energy between liquid and solid phases and at sufficient rapid cooling rates, the metastable phase is retained at room temperature.[18–20] In addition, it has to be noticed that the metastable phase observed (the γ phase with a cubic close packing of oxygen ions, e.g. spinel lattice) has a structure closer to that of the liquid which is assumed to have a tetrahedral co-ordination of aluminium by oxygen rather than the hexagonal packing of α-Al_2O_3. The amount of α-Al_2O_3 still identified is probably indicative of the presence of unmelted and/or recrystallised particles (due to low cooling rate) in the coating.

According to the XRD patterns of the multi-oxide coatings, the γ-Al_2O_3 phase was not detected even

Fig. 6. Example of 'free-flight' particles, where the melting stage is more or less completed (Ar:He, 16.5 kW, 7 l min^{-1}).

though long searches were performed in the 20–50° (2θ) zone. The XRD analysis seems to show that the same volume of α-Al_2O_3 is converted either to γ-Al_2O_3 in the pure alumina coating or to Zn_4 and SPI in the oxide mixture deposit. The whole XRD results seem to show that the elementary components are so intimately mixed that, as soon as alumina particles are melted a complete chemical reaction occurs to form SPI and/or Zn_4 even though the flying time in the reaction zone is short.

At a fixed plasma power, in the Ar:He plasma, the granules with a size over 36 μm undergo a peripheric melting which leads to the formation of a gangue (Fig. 7a). In contrast, granules treated in an Ar:H_2 plasma seem to be fully melted (Fig. 7b). Moreover, it has been found that the α-Al_2O_3 phase is of major importance in the case of an Ar:He plasma whereas the Zn_4 and SPI phases are predominant in an Ar:H_2 plasma (Fig. 7c) which is in good agreement with the SEM observations previously reported.

These phenomena arise from the differences in thermal properties of Ar:H_2 and Ar:He plasma mixtures. An observation of the temperature evolution along the plasma jet axis (Fig. 8) for both plasma mixtures (Ar:H_2 and Ar:He) clearly shows that powder is submitted to similar temperatures. However, it is well known that the thermal conductivity is higher for the Ar:H_2 mixture for

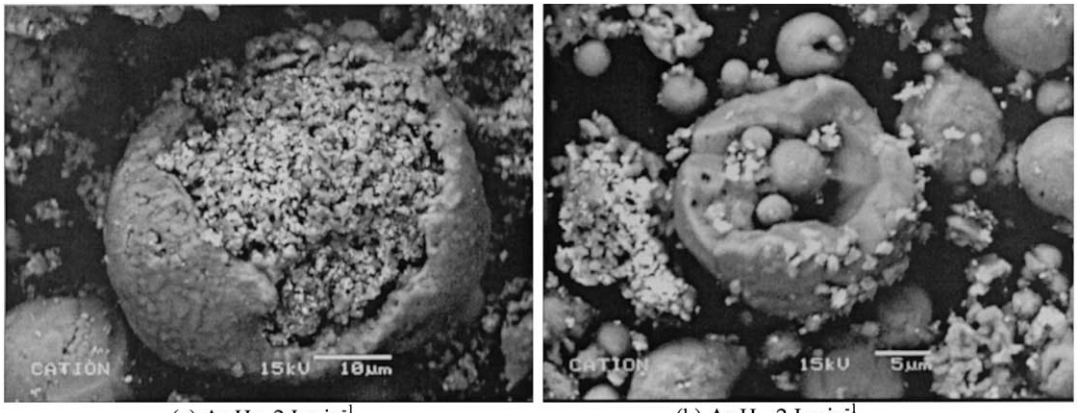

(a) Ar:He, 2 Lmin^{-1} (b) Ar:H_2, 2 Lmin^{-1}

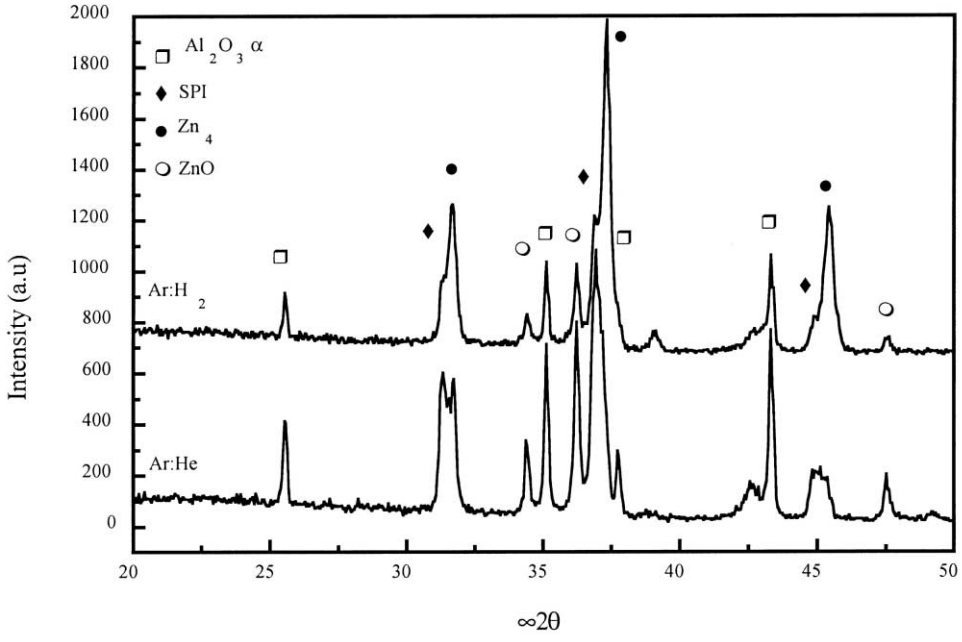

(c) XRD patterns versus composition of plasma gas

Fig. 7. Morphology of the powder particles after passing through the plasma jet as a function of the plasma gas nature (identical carrier gas flow rate of about 2 l min^{-1} and plasma jet power around 16.5 kW) and corresponding XRD diffraction patterns.

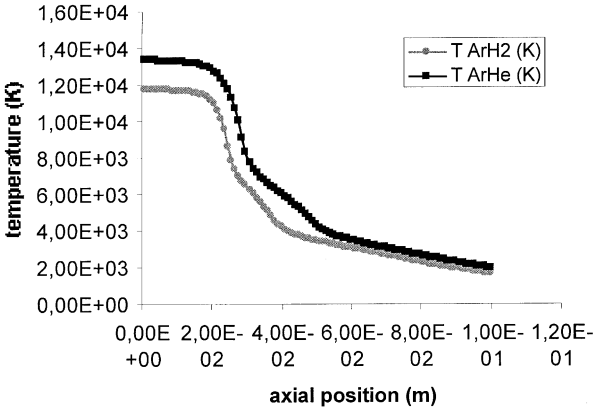

Fig. 8. Evolution of the temperatures along the plasma jet axis versus nature of the plasma (Ar:H_2 or Ar:He for a plasma power of 16.5 kW).

temperatures $T > 3000$ K with a peak around 3700 K[21] which will enhance the thermal transfer from the gases to the powder.

Whatever the nature of the plasma, for a plasma power of 16.5 kW, the powder melting is not completely achieved and depends highly on the particle size. However, an increase of the power of about 35% leads to an increase in the amount of melted particles leading to complete reaction between the components to form SPI and Zn_4 which has been observed on the XRD pattern (Fig. 5).

By choosing the plasma characteristics and the aggregate size, one can achieve different ways of powder melting, i.e. either a superficial one leading to the formation of a gangue or a bulk one leading to a homogeneous grain. Of course, this depends highly on the particles trajectory that is itself a function of the carrier gas flow rate. Due to its lower density, an agglomerated non-sintered powder is probably more sensitive than a conventional powder to the properties of a plasma jet such as viscosity (the viscosity of the Ar:He plasma is higher (2.5 times at 15 kK and 1.5 times at 10 kK) than that of the Ar:H_2 plasma,[21]). So, an agglomerated non-sintered powder will need higher initial momentum at the injector exit to reach the hot zones of the plasma.

For both compositions of plasma and for an identical plasma power, an increase in the carrier gas flow rate leads to better melting combined with a reduction of the mean final granule size as reported in Fig. 9 (for instance, in an Ar:H_2 plasma, the granule diameter decreases from 12 to 6 μm when the carrier gas flow rate increases from 2 to 7 l min^{-1}). The studies of the powder impact location relative to the plasma jet axis and of the amount of material transferred to the substrate demonstrated that there is an optimum value of the carrier gas flow rate. Indeed, the axial deviation (which represents the distance between the plasma jet axis and the powder impact) increases with the carrier gas flow rate from 2 mm for 3.5 l min^{-1} to 9 mm for 9 l min^{-1} while the deposition yield passes through an optimum value (around 75%), which is achieved around 5 l min^{-1} for a 36–63 μm size range.

In conclusion, the degree of the reaction between Al_2O_3 and ZnO/MgO depends highly on the melting stage, which is a function of the nature of the plasma, the power and the carrier gas flow rate.

$$\underset{(675\ \text{Å})}{\alpha\text{-}Al_2O_3} + MgO + ZnO \longrightarrow \underset{1860\ \text{Å}}{\alpha\text{-}Al_2O_3}$$

$$+ \underset{(325\ \text{Å})}{Zn_4Al_{22}O_{37}}\ \text{or/and}\ \underset{(450\ \text{Å})}{(Mg/Zn)Al_2O_4}\ \text{grain size}$$

3.3. Coating build-up

The melting degree of spray-dried granules has not only an influence on the crystalline changes but also on the splat spreading and consequently on their stacking

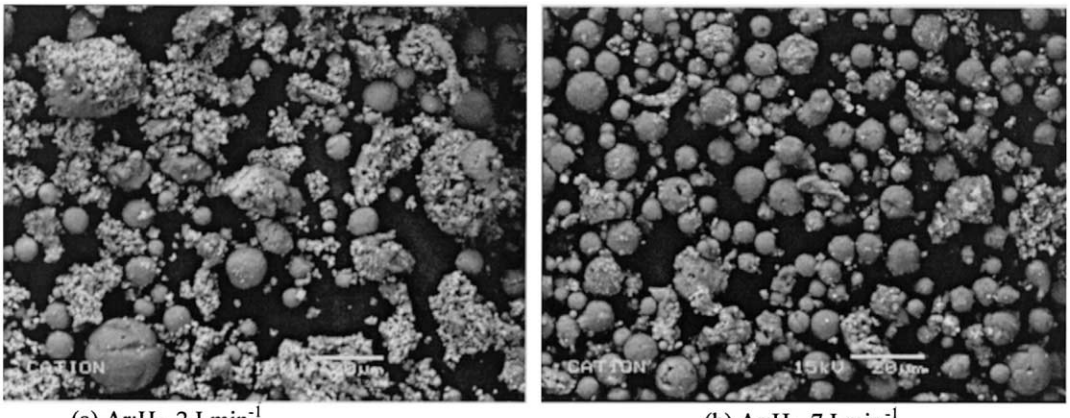

(a) Ar:H_2, 2 $Lmin^{-1}$ (b) Ar:H_2, 7 $Lmin^{-1}$

Fig. 9. Evolution of the powder particles after passing through the plasma jet as a function of the carrier gas flow rate in an Ar:H_2 plasma (plasma power fixed at 20.5 kW).

mode and finally on the coating characteristics. To evaluate this influence, experiments and morphological analysis were conducted on

- particle impacts performed by moving rapidly the torch in front of a polished substrate at ambient temperature,
- deposits, studied either on or after being removed from the substrate.

3.3.1. Splat spreading

The observations of the splats after individual particle impact on the substrate lead to same conclusions as those drawn from the free-flight powder analysis. It appears in general that granules are more melted in an $Ar:H_2$ plasma than in an Ar:He plasma. Indeed, for an Ar:He plasma, numerous small angular particles are observed (Fig. 10a) corresponding to the Al_2O_3 initial grains. In contrast, for an $Ar:H_2$ plasma (Fig. 10b), dense homogeneous spherical particles (average diameter about 1.5 μm) having undergone a change of state during spraying, can be viewed. In both cases, on top of the presence of these small particles, big aggregates around 30–40 μm in diameter have impacted on the substrate showing a partial melting. The outer part of these aggregates seems to be fully melted which allows the granules to stick to the substrate whereas the inner part sometimes remains unmelted (Ar:He) or appears to be strengthened by local sintering ($Ar:H_2$).

An increase in the carrier gas flow rate, as previously observed for the free-flight powder analysis, leads to a better melting of the aggregates. More precisely, in an $Ar:H_2$ plasma, it can be observed at 7 l min^{-1} (Fig. 11a) that core melted particles with size in the range 5–10 μm are much more numerous than at 3.5 l min^{-1} (Fig. 10b). Another means to enhance the melting of the aggregates is to introduce the powder with an angle of 70° instead of 90°, which forces the particles to cross the hottest zone of the plasma jet. In these conditions, when the droplets touched the substrate they were smeared out as they solidified. The result was the formation of solidified fingers around the bulk of the splats as seen on Fig. 11b. Solidification seems meanwhile to be fast enough to arrest spreading rapidly after impact. These observations are in accordance with numerical and other experimental results[22] performed with conventional powder (agglomerated/sintered). In the present case the splats are smaller in size.

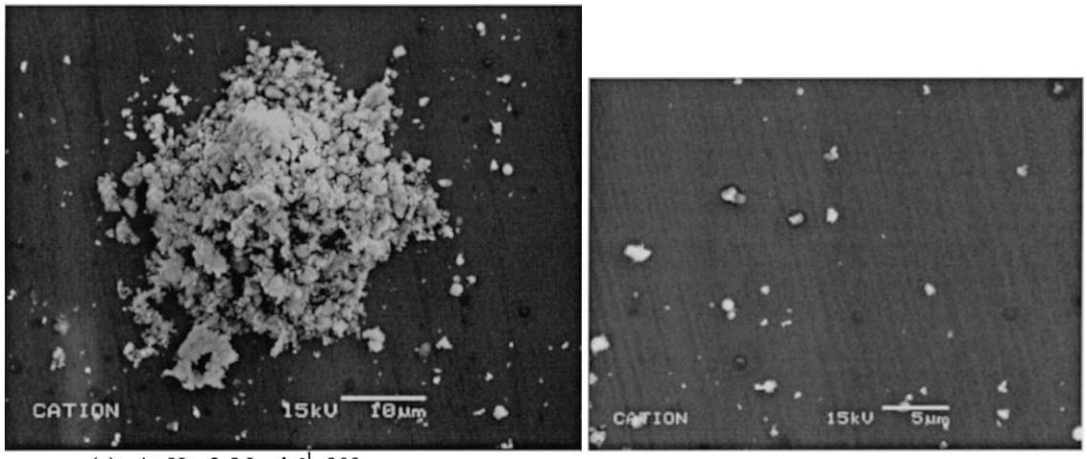

(a) Ar:He, 3.5 $Lmin^{-1}$, 90°

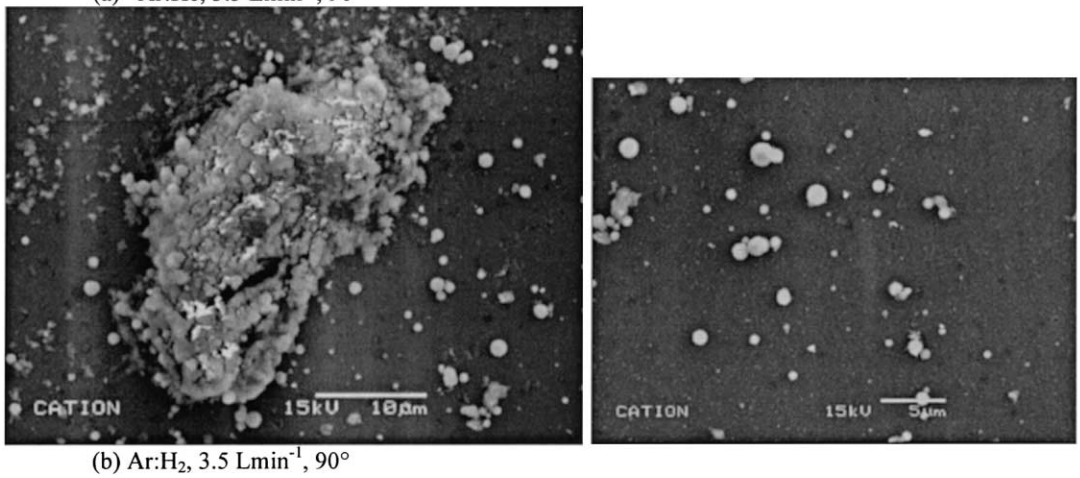

(b) $Ar:H_2$, 3.5 $Lmin^{-1}$, 90°

Fig. 10. Evolution of the powder splats versus the nature of the plasma at a power of 20.5 kW.

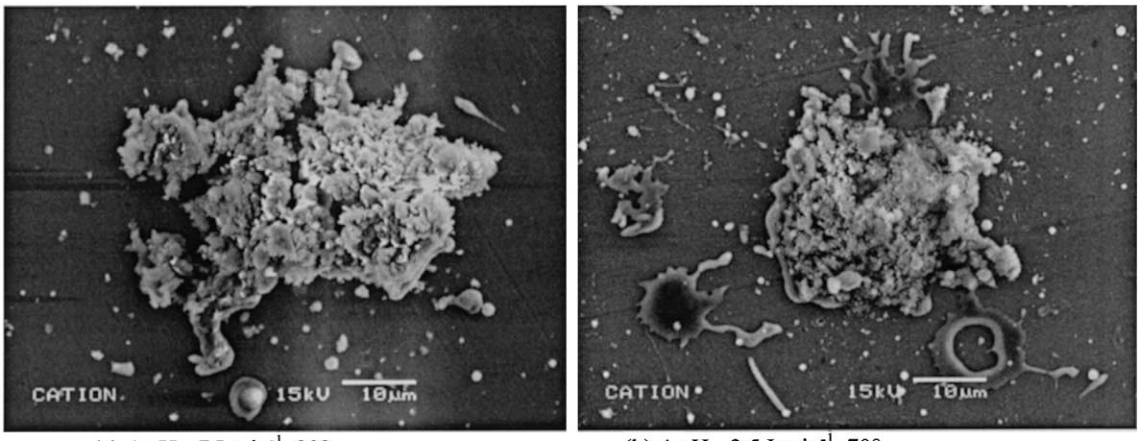

(a) Ar:H_2, 7 Lmin^{-1}, 90° (b) Ar:H_2, 3.5 Lmin^{-1}, 70°

Fig. 11. Evolution of the powder splats as a function of the carrier gas flow rate and powder injection angle for an Ar :H_2 plasma at a power of 20.5 kW.

In general, it appears from this study of particles impact that:

- small fully melted splats are formed whose size depends on the operating conditions
- inside an aggregate, the components can stay non melted
- the outer parts of the aggregates are always melted so the granules and splats can stick all together which is supposed to lead to a cohesive non-powdery coating.

3.3.2. Coating characteristics

The coatings show a layered structure due to the splat spreading with many cavities when observed by SEM (Fig. 12). The splat shape depends on the process conditions. Indeed, when the plasma is more energetic (nature and/or power changes), the particle spreading is enhanced. For example, in an Ar:H_2 plasma, the splat thickness varies from 0.6 to 1.5 μm for a low power (16.5 kW) to 0.35 to 0.6 μm for a high power (22.5 kW) which is a far less than the conventional average splat thickness (5 μm). This phenomenon is also indicated by the roughness value R_a. Depending on the powder size range, the roughness varies between 8.1 ± 0.1 μm for a coating sprayed with an Ar:He plasma and with a 36–63 μm powder fraction to 3.8 ± 0.1 μm for a deposit sprayed from an Ar:H_2 plasma and a -36 μm powder fraction. It has to be noticed that these roughness values are lower (60%) than the ones generally recorded for standard ceramic sprayed coating. As the melting step is not entirely completed, the porosities and cavities are quite numerous. A variation of MIP (mercury intrusion porosimetry), namely the so-called Archimedes method, in which the sample is infiltrated by water at atmospheric pressure was applied in order to determine the true porosity of the coatings. The densities were calculated from the difference between the weight of the sample in air and in water. It appeared that the maximum apparent packed density of about 3.6 g cm^{-3} is achieved when the melting stage of the whole particle size range was optimised (Ar:H_2/20.5 kW/3.5 l min^{-1}/

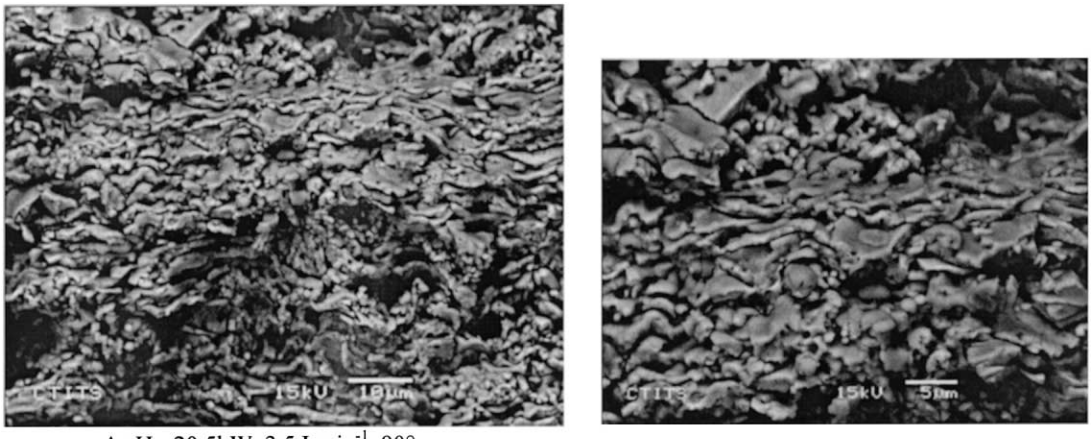

Ar:H_2, 20.5kW, 3.5 Lmin^{-1}, 90°

Fig. 12. Coating morphology observed by SEM on cross-sections.

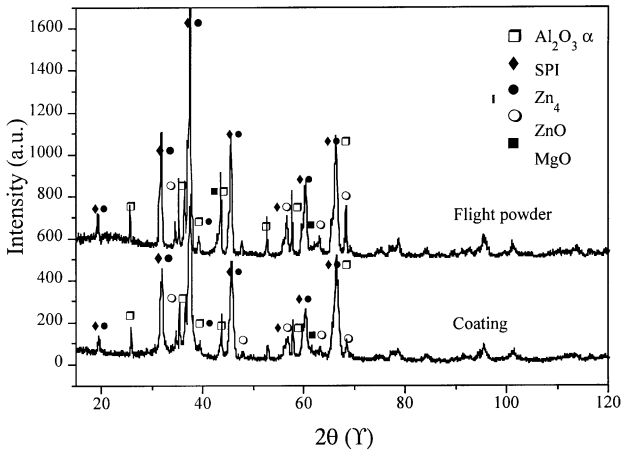

Fig. 13. Diffraction patterns of a free-flight powder and corresponding coating (Ar:H_2, 20.5 kW, 3.5 l min^{-1}) in $\theta/2\theta$ mode.

70°). On the basis of the major crystallographic composition of this coating, the porosity is evaluated to be about 15%.

XRD studies show that the patterns recorded with the 'free-flight' powders and the corresponding coatings (Fig. 13) are identical as far as the crystalline phases are concerned. This indicates clearly that the chemical reactions occur during the plasma crossing. However, noticeable peak widening for SPI and Zn_4 is recorded in the coating pattern as compared to the pattern for the corresponding powder. Whereas the evaluated crystallite size is relatively unchanged from the powder to the coating (respectively about 450Å for SPI and 280Å for Zn_4), the broadening of the reflection peaks can be attributed to an increase in the strain due to the coating build up or to a deviation from stoichiometry.[23] Variations in relative intensities and peak positions are very difficult to attribute because of variations in coating roughness, strains (stoechiometry, crystallite defaults...) and grain size. As a consequence, by varying the deposition parameters few explicable crystallographic differences were noticed.

4. Conclusion

A non-conventional method of plasma spraying ceramics (named DPPS) using non-sintered spray dried aggregates as starting materials was investigated. The deposits obtained from the elementary oxides: Al_2O_3, MgO and ZnO had a thin layered structure. It was demonstrated that the morphology and chemical composition of the splats produced are heavily dependent on both the plasma characteristics (nature and power) and the powder injection parameters (carrier gas flow rate and injector angle).

Due to the very fine mixing of the elementary powders, the starting oxides react together to form spinel ($MgAl_2O_4$ and/or $ZnAl_2O_4$) and zinc aluminum oxide ($Zn_4Al_{22}O_{37}$) phases. The SPI and Zn_4 phases seem to take the place of the γ-Al_2O_3 phase that would have been formed in the case of a pure alumina coating. This demonstrates that the elementary components are so intimately mixed that as soon as they melt they can react. Simultaneously, this seems to indicate that the aggregates are not totally broken up when entering in the plasma jet.

The plasma spray synthesis is a single-step process. Depending on the operating conditions, the chemical reaction is driven to different degrees of completion during the spray processing itself, resulting in the formation of a cohesive non-powdery coating. By reducing the size of the starting aggregates, a roughness (R_a) as low as 3.8 μm can be achieved for a 200 μm thick coating. Finally two different types of splats were identified: the first one consisting of individual well-melted droplets and the second of the starting aggregates melted at their outer parts and just strengthened in their cores. The former is dominant in an Ar:H_2/70° plasma leading to dense coatings built of 1 μm thick splats whereas the latter is dominating in an Ar:He/90° plasma leading to porous coatings.

Acknowledgements

The authors are grateful to Serge Vives from the CREST laboratory for assistance in XRD experiments and to Christine Clément from CATION for the SEM observations. The help of F. Tourenne for powder fabrication is acknowledged. Thanks go to R. Bolot for plasma temperature calculations.

References

1. Ilavsky, J., Long, G. G., Allen, A. J., Herman, H. and Berndt, C. C., Use of small-angle neutron scattering for the characterization of anisotropic structures produced by thermal spraying. *Ceramics*, 1998, **42**(3), 81–89.
2. Herman H. and Sampath S., *Thermal Spray Coatings in Metallurgical and Ceramic Protective Coatings*, ed. K.H. Stern, Chapman & Hall, London, 1996, pp. 261–289.
3. Bonneau, M., Gitzhofer, F. and Boulos, M., SOFC/CeO_2 doped electrolyte deposition using suspension plasma spraying. In *Thermal Spray, Surface Engineering via Applied Research*, ed. C. C. Berndt. ASM Int., ITSC', Montréal, Canada, 2000, pp. 929–934 8–11 May 2000.
4. Blazdell, P. and Kuroda, S., Plasma spraying of submicron ceramic suspensions using a continuous ink jet printer. *Surf. & Coat. Technol.*, 2000, **123**, 239–246.
5. Karthikeyan, J., Berndt, C. C., Tikkanen, J., Wang, J. Y., King, A. H. and Herman, H., Nanomaterials powders and deposits prepared by flame spray processing of liquid precursors. *NanoStructured Materials*, 1997, **8**(1), 61–74.
6. Tikkanen, J., Gross, K. A., Berndt, C. C., Pitkanen, V., Keskinen, J., Raghu, S., Rajala, M. and Karthikeyan, J., Characteristics of

the liquid flame spray process. *Surf. & Coat. Technol*., 1997, **90**, 210–216.
7. Karthikeyan, J., Berndt, C. C., Reddy, S., Wang, J. Y., King, A. H. and Herman, H., Nanomaterial deposits formed by DC plasma spraying of liquid feedstocks. *J. Am. Ceram. Soc*., 1998, **81**(1), 121–128.
8. De Arellano-Lopez, A. R. and Faber, K. T., Microstructural characterization of small-particle plasma spray coatings. *J. Am. Ceram. Soc*., 1999, **82**(8), 2204–2208.
9. Lallemand, G., Fayeulle, S. and Treheux, D., Fabrication process of spinel powder for plasma spraying. *J. Eur. Ceram. Soc*., 1998, **18**, 2095–2100.
10. Petot, C., Ducos, M. and Petot-Ervas, G., Thermal spray spinel coatings on steel substrates: influence of the substrate composition and temperature. *J. Eur. Ceram. Soc*., 1995, **15**, 637–642.
11. Grutzner, H. and Weiss, H., Development of ceramic plasma sprayed coatings against slag attack for steel industry. In *Advances in thermal spraying*. Pergamon Press. Montreal, 1986, pp. 349–357.
12. Nakamichi, M., Kawamura, H., Miyajima, K., Harada, Y. and Oyamada, R., Trial fabrication and preliminary characterization of $MgO{\cdot}Al_2O_3$ coating. *J. Nucl. Mater*., 1996, **233-237**, 1427–1430.
13. Wang, H. G. and Herman, H., Structure and properties of plasma-sprayed spinel. *Ceramic Bulletin*, 1989, **68**(1), 97–102.
14. Masters K., *Spray Drying Handbook*, 4th edn, Longman Scientific & Technical.
15. Gourlaouen, V., Hansz, B., Remy, F. and Coddet, C., *Thermal Spray, Meeting the Challenges of the 21st Century*, ed. C. Coddet. ASM Int., Montréal, 1998, pp. 1293-1297.
16. Kingon, A.I., Davis, R.F. and Thackeray, M.M., Engineering properties of multicomponent and multiphase oxides. In *Engineered Materials Handbook,* Vol. 4, *Ceramics & Glasses*, ed. ASM, 1991, pp. 758–774.
17. Santhiya, D., Subramanian, S., Natarajan, K. A. and Malghan, S. G., Adsorption and electrokinetic studies on alumina suspensions using poly(vinyl alcohol). *Minerals Metall. Process*, 1999, **16**(2), 51–55.
18. McPherson, R., Formation of metastable phases in flame and plasma prepared alumina. *J. Mater. Sci*., 1973, **8**, 851–858.
19. Erickson, L. C., Troczynski, T., Hawthorne, H. M., Tai, H. and Ross, D., Alumina coatings by plasma spraying of monosize sapphire particles. *J. Therm. Spray Technol*., 1999, **8**(3), 421–426.
20. Vardelle, A., Robert, C., Wang, G. X. and Sampath, S., Analysis of nucleation, phase selection and rapid solidification of an alumina splat. In *Thermal Spray, Meeting the Challenges of the 21at Century*, ed. C. Coddet. ASM Int, Montréal, 1998, pp. 635–643.
21. Pateyron, B., Elchinger, M.-F., Delluc, G. and Fauchais, P., Thermodynamic and transport properties of Ar-H_2 and Ar-He plasma gases used for spraying at atmospheric pressure. I: properties of mixtures. *Plasma Chemistry and Plasma Processing*, 1992, **12**(4), 421–448.
22. Pasandideh-Fard, M., Mostaghimi, J. and Chandra, S., Numerical simulation of thermal spray coating formation. In *Thermal Spray, Surface Engineering via Applied Research*, ed. C. C. Berndt. ASM Int., ITSC', Montréal, Canada, 2000, pp. 125–134 8–11 May 2000.
23. Jing, S.-Y., Lin, L-B., Huang, N.-K., Zhang, J. and Lu, Y., Investigation on lattice constants of Mg–Al spinels. *J. Mater. Sci. Letts*., 2000, **19**, 225–227.